Structural Colors from Fano Resonances

Yichen Shen,*[†,‡,⊥] Veronika Rinnerbauer,[†,§,⊥] Imbert Wang,[†] Veronika Stelmakh,[†] John D. Joannopoulos,[†,‡] and Marin Soljačić[†,‡]

[†]Institute For Soldier Nanotechnologies, Massachusetts Institute of Technology, Cambridge, Massachusetts 02139, United States
[‡]Department of Physics, Massachusetts Institute of Technology, Cambridge, Massachusetts 02139, United States
[§]Institute of Semiconductor and Solid State Physics, Johannes Kepler University, Linz, Austria

S Supporting Information

ABSTRACT: Structural coloration is an interference phenomenon where colors emerge when visible light interacts with nanoscopically structured material and has recently become a most interesting scientific and engineering topic. However, current structural color generation mechanisms either require thick (compared to the wavelength) structures or lack dynamic tunability. This report proposes a new structural color generation mechanism that produces colors by the Fano resonance effect on thin photonic crystal slab. We experimentally realize the proposed idea by fabricating the samples that show resonance-induced colors with weak dependence on the viewing angle. Finally, we show that the resonance-induced colors can be dynamically tuned by stretching the photonic crystal slab fabricated on an elastic substrate.

KEYWORDS: structural colors, Fano resonance, tunable colors, photonics crystals, optical coatings, surface structure
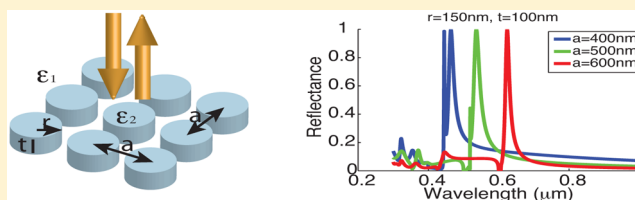
People have long been inspired by nature's ability to create a dazzling range of colors. Dyes, pigments, and metals that absorb light of only certain colors and reflect the rest of the spectrum are the most common color generation mechanisms. Recently, great attention has been paid to a different type of color generation mechanism: structural coloration, which produces color without the use of dyes and pigments.[1] Structural coloration is, in principle, an interference phenomenon where colors emerge when visible light interacts with nanoscopically structured material. Compared with pigmentary colors, structural colors (1) usually appear brighter under sunlight; (2) are immune to photobleaching, and (3) can be tuned dynamically.[2] Because of those advantages, they have found applications in painting, textiles, and passive displays.[3,4]

Structural colors are typically produced by light interference within bulk materials, for example, structural colors from scattering,[5−7] multilayer interference,[8−10] and photonic crystals.[4,11−13] In these bulk effects, the color gets brighter and sharper as one increases the bulk thickness, i.e., number of particles (for scattering), the number of layers (for multilayer interference), or the number of periods (for photonic crystals). As a result, designs based on these mechanisms require the structured materials to be much thicker than the wavelength. However, in certain applications, such as optical coating,[14,15] structures with low thickness are preferred.[16] Conventional optical coatings use thin film interference, which typically requires metallic substrates in order to achieve enough reflection. Therefore, the structural colors generated through thin film interference are material limited, angular selective and cannot be tuned dynamically. Recently, structural colors from plasmonic effect was investigated extensively.[17−24] It has

demonstrated promising features including low thickness (single layer structure), full color display, and friendly for nanofabrication. However, since metals inherently lose in the visible spectrum, the reflection peak from plasmonic effect is typically broadband and less intensive. Furthermore, plasmonic colors are also angular sensitive.

In this letter, we propose a new mechanism to generate structural color, different from any of the current mechanisms mentioned above, that produces color by interference between the directly reflected light and the guided resonances mode on a *surface structure*. The new mechanism exhibits strong peak reflection (100% in simulation), is flexible in material choice, is suitable for large area fabrication, and has weak angular dependence. Moreover, it supports dynamic tuning of the reflectance spectrum, as we will demonstrate in this study.

The resonance-induced reflectance used in this study to generate static and dynamic color is related to a more general resonance category, known as Fano resonance.[25] This optical resonance was first investigated and analyzed by Fan et al.[26] in photonic crystal slabs. The optical Fano resonance can be understood as an interference effect: light incident on a periodic surface structure (Figure 1a) excites a one-dimensionally confined mode supported by the surface structure. The localized mode leaks into the surrounding environment (Figure 1d), interfering with the directly reflected light from the surface. When the reflected and the radiated light have the same phase, constructive interference produces a sharp reflectance peak (Figure 1b,c). The reflectance line shape near resonance peak
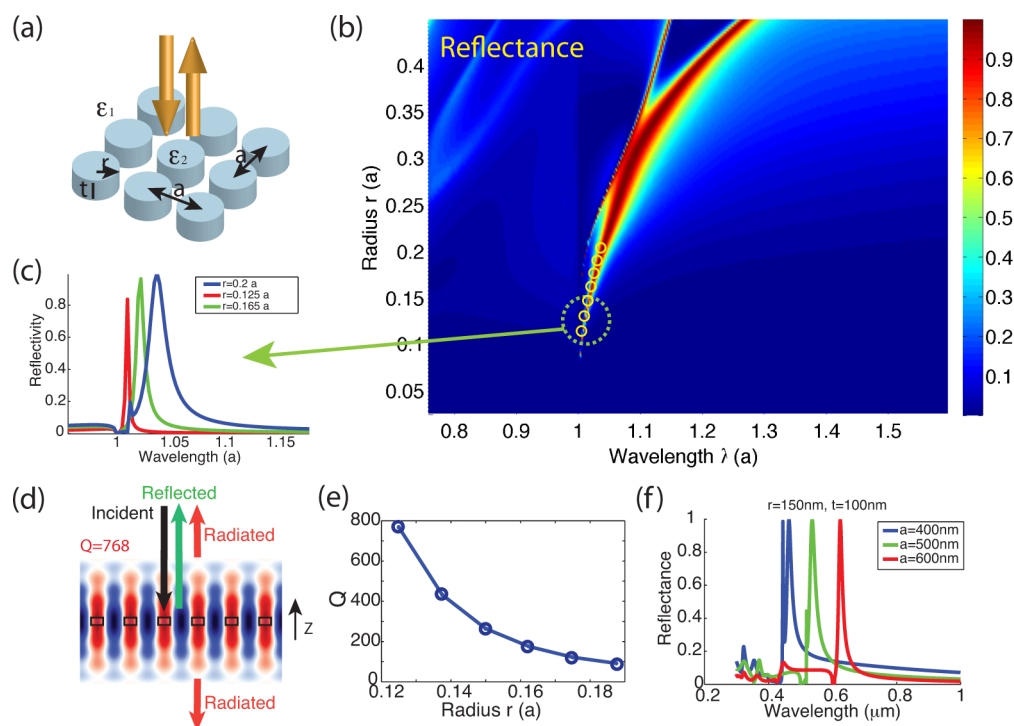
Figure 1. Light reflectance assisted with Fano resonance. (a) Light with random polarization incident on a periodic array of nanorods. The dielectric constant of the nanorods is set to be $\varepsilon_2 = 4$ (Ta_2O_5) and the surrounding medium $\varepsilon_1 = 1$ (vacuum). (b) Reflectance spectra versus different radii r of the rods with height $t = 0.25a$. The reflectance peaks are the result of interference between the directly reflected light and radiated light from the resonant modes. The yellow rings correspond to the locations of the theoretically simulated resonant modes. (c) Example of reflectance peaks caused by Fano resonance for structures with $r = 0.125a$, $r = 0.165a$, and $r = 0.2a$. (d) Vertical slice of the spatial distribution of the electric field for the resonant mode responsible for the reflectance peak with $r = 0.125a$ in panel c. (e) Q values for the resonance modes versus the rod radius. (f) Shift of the reflectance peak when periodicity a is varied, while the rod radius $r = 150$ nm and rod height $t = 100$ nm are fixed.

can be calculated by temporal coupled mode theory and fitted by the line shape:[27]

$$r = r_\mathrm{d} + f \frac{\gamma}{\mathrm{i}(\omega - \omega_0) + \gamma} \quad (1)$$

where the factor f is the complex amplitude of the resonant mode, r_d is the direct reflection coefficients, and ω_0 and γ are the center frequencies and widths of the resonance, which are directly related to the quality factor Q of the resonance mode:

$$Q \approx \frac{\omega_0}{\gamma} \quad (2)$$

To date, most Fano resonance features discussed have a rather high Q (>50) to be used for lasing or filtering purposes. In these cases, the reflectance peak is a relatively narrow band. However, in order to achieve color control using Fano resonance, the reflectance peak needs to be reasonably broadband to reflect enough light. As a proof of principle, we study a square lattice of rods as shown in Figure 1a. This structure is also chosen for its suitability for dynamic tuning, which will be discussed later in this letter. The dielectric constant of the rods is chosen to be $\varepsilon_2 = 4$ (e.g., Ta_2O_5), and the surrounding environment has $\varepsilon_1 = 1$, i.e., vacuum. The reflectance spectra for structures with different rod radii r are computed with the rigorous coupled wave analysis (RCWA) method[28] and plotted in Figure 1b. The bandwidth of the resonant peaks increases with increasing radius r of the rods. The resonant modes at different r and the corresponding field distribution are calculated using a finite difference time domain (FDTD) method[29] (Figure 1d), and their locations are

highlighted in Figure 1b. The spectral position of the resonant modes exactly follows the reflectance maxima, suggesting that the reflectance peaks are indeed caused by Fano resonance. The quality factor Q for each resonant mode is evaluated using a low-storage filter diagonalization method (FDM)[30] and plotted in Figure 1e, which shows that Q decreases as r increases.

One interesting feature of Fano resonance induced reflection spectrum is its angular dependence. Since the location of the reflection peaks strictly follow the resonance modes inside the photonics crystal (PhC) slab, under certain conditions (see Supporting Information), the reflection peak can be designed to have very weak angular dependence. Such near-omnidirectional reflective color is hardly observed in other structural coloration mechanisms and would be useful in many applications.[31,32]

Furthermore, since the resonant mode of the photonic crystal is directly related to the periodicity of the lattice, one can actively tune the location of the reflection peak simply by changing the period a of the structure (Figure 1f).

As a proof of concept, we first realize samples that have resonance-induced, *static* color in the red-to-NIR regime. In the next step, we experimentally realize the same structures on elastic substrates (PDMS) and demonstrate their *dynamic* tunability by varying the periodicity a.

The target structure to achieve Fano resonance consists of rods of a high-index material (Si) on a transparent substrate. In our first experiment, the structures proposed in Figure 1 were fabricated on amorphous SiO_2 (glass) substrates, with two different periods of 450 and 500 nm, radius from $r = 115$ to $r = 125$ nm, and height $t = 65$ nm. The radius and the thickness of the rods were optimized to support a resonant mode with a Q
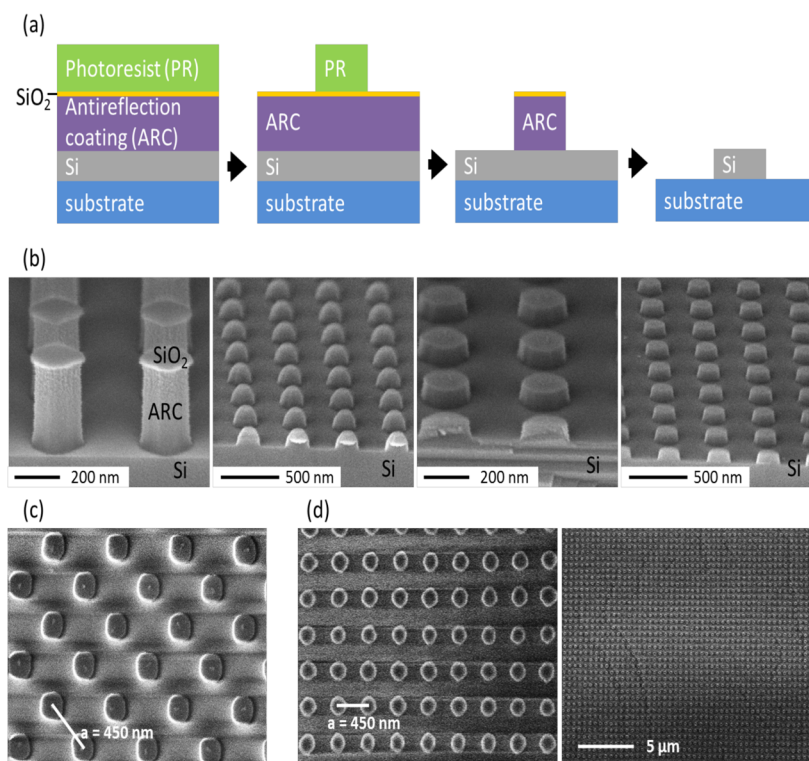
Figure 2. Fabrication process. (a) Schematic outline of the process flow: Deposition of the Si layer and lithography layers, pattern definition by interference lithography , and pattern transfer by RIE. (b) Scanning electron micrographs of the process steps: Sample after RIE of the ARC, after RIE of the Si layer, and after ashing of the remaining ARC (from left to right); cross sections are taken from test samples on Si substrates. (c) Final Si rods on glass substrates and on (d) PDMS.

low enough to produce a significant color effect. In order to get a good optical effect, it is critical that the rods have a high index of refraction while having low absorptivity. That is why amorphous Si was used for the rods.

For the static color samples, fused silica substrates were cleaned and a layer of 65 nm of Si was deposited by plasma enhanced chemical vapor deposition (PECVD) at a substrate temperature of 200 °C. The refractive index and thickness of the Si layer were confirmed by spectroscopic ellipsometry to be $n = 4.3$ at 600 nm and 4.0 at 700 nm, while the imaginary part is below $\kappa = 0.4$ at 600 nm and vanishes at 700 nm.

The fabrication process of the periodic structures was based on interference lithography (IL) using a trilayer process[33,34] as shown in Figure 2. IL is a relatively inexpensive, fast, and scalable maskless lithography method, which relies on the interference pattern generated by two coherent light sources to define 1D and 2D periodic patterns in a single plane and is easily scalable to large exposure areas. The lithography layer stack consisted of an antireflective coating (AZ BARLi, 200 nm), a thin layer of SiO$_2$ (20 nm, deposited by electron beam evaporation) to protect the antireflective coating (ARC) during reactive ion etching (RIE), and PFi-88 (Sumika, 200 nm) as a negative photoresist. The IL was done using a Lloyd's mirror setup with a 325 nm HeCd Laser. The periodicity of the pattern is defined by the interference angle, and the exposure was performed twice, with the substrates rotated by 90° between exposures to create a square array of cylindrical rods in the negative resist. After development of the photoresist and RIE of SiO$_2$ and ARC, the pattern was transferred to the Si layer by RIE using CF$_4$/O$_2$ chemistry. In the end, the remaining ARC was removed by plasma (O$_2$) ashing.

The fabricated sample appeared red in color over a wide range of viewing angles (Figure 3c). The reflectance of the samples at different incident angles was measured using an ultraviolet−visible spectrophotometer (Cary 500i). In Figure 3b we show that the reflection peaks indeed depend weakly on the incident angles, as discussed above. Clearly there is a resonance band around 650−700 nm for small angles, which decreases for angles <10°, while there is another resonance band contributing for angles >20° in the wavelength around 650 nm. The resulting reflection spectrum consists of two different resonance bands, which allow us to observe similar resonant reflectance color for a wide range of angles (similar to the effect in the Supporting Information). The reflectance spectra at normal incidence of samples fabricated with different periodicity a and rod radius r are shown in Figure 3d. The resonance wavelength clearly increases as r and a increase as predicted. Compared with the RCWA simulation result (dashed line), the experimental Fano reflectance peaks are broadened due to the nonradiative loss in the structure, possibly due to material absorption and fabrication inaccuracies, in particular local variations in the geometry. Nevertheless, we observed a 3-fold increase in sample's reflectance around the resonance wavelength. Because of the dramatic increase of the absorption in amorphous Si at smaller wavelengths, this particular structure's Fano resonance effect can only be observed at wavelengths longer than 600 nm. However, with suitable lossless materials one should be able to demonstrate this effect also in the lower wavelength regime.

In our second experiment, we demonstrated dynamic color tuning using the same Fano resonance mechanism. In order to achieve the desired effect, the structures were fabricated on polydimethylsiloxane (PDMS) substrates (Figure 4) instead of
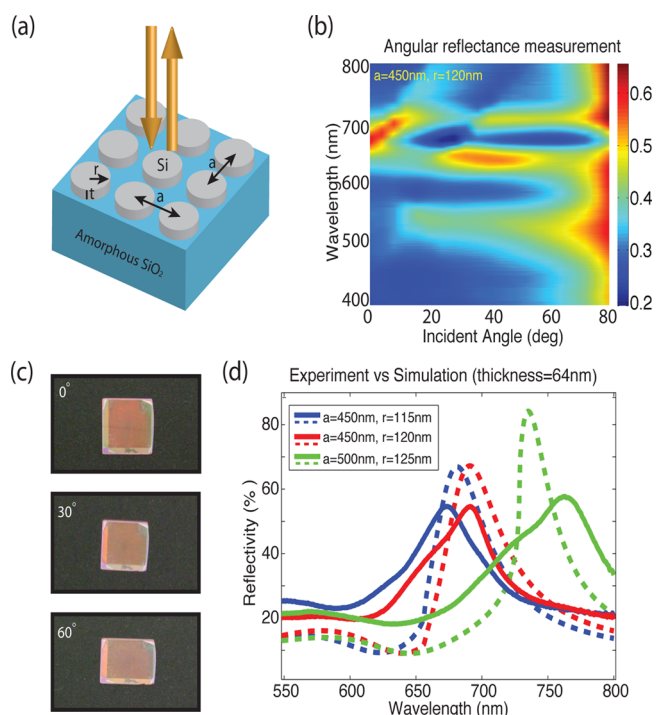
Figure 3. Si rods on amorphous silica wafer. (a) Illustration of the simulated and fabricated structure. (b) Measured reflectance spectra of a sample with $a = 450$ nm and $r = 120$ nm over all viewing angles. (c) Photographs of the fabricated sample with $a = 450$ nm and $r = 120$ nm at different viewing angles. The sample's color appeared red irrespective of the viewing angles (rod structure in the center, edge area only partially exposed due to lithography setup). (d) Experimental demonstration of color control: Measured (solid lines) and simulated (dashed lines) reflectance spectra of structures with different geometries of the periodic Si rods fabricated on amorphous silica substrates.

Figure 4. Si rods on PDMS. (a) Illustration of the simulated and fabricated structure. (b) The periodicity a of the rod lattice can be adjusted by stretching the PDMS. In order to simulate isotropic stretching, the sample is fixed on a balloon, which is gradually blown up. (c) Dynamic color control: Measured (solid lines) and simulated (with ideal structure, dashed lines) reflectance spectra of silicon rods with $a = 450$ nm and $r = 100$ nm on polydimethylsiloxane (PDMS) before and after stretching by 10%.

glass substrates. To this end, PDMS (Sigma-Aldrich, approximately 200 μm thick) was spin-coated on 5 cm silanized Si wafers and annealed at 150 °C for 30 min. The Si substrates serve as a support in nanofabrication and can be removed afterward by peeling off the thick PDMS layer. The PDMS was surface treated by O$_2$ ashing (200 W) to enhance adhesion and resistance to wet chemical processing, which resulted in some surface damage and macroscopic cracking in the PDMS surface. On the prepared PDMS substrates, a layer of 65 nm of Si was deposited by PEVCD at a substrate temperature of 150 °C.

The fabrication process of the Si rods on the prepared PDMS substrates was similar to that on the glass substrates. To achieve higher fabrication accuracy, a Mach−Zehnder setup was used for the IL on the PDMS substrates, instead of the Lloyd's mirror.[35−37]

In the fabrication process it must be taken into account that PDMS is temperature sensitive and elastic and also highly sensitive to wet chemical processing. While the deposition of Si on glass was straightforward, the PECVD on PDMS resulted in a dull Si surface, on which the cracks from ashing were plainly visible, with considerable surface roughness visible under a microscope. Nevertheless, the Si layer on PDMS appears to be a sufficiently flat layer on a nanoscopic scale, and the optical properties are close to those of amorphous Si. As a result of the difficult fabrication process on the elastic substrates, the achieved structures have an acceptable nanoscopic accuracy (Figure 2), but rather low macroscopic uniformity.
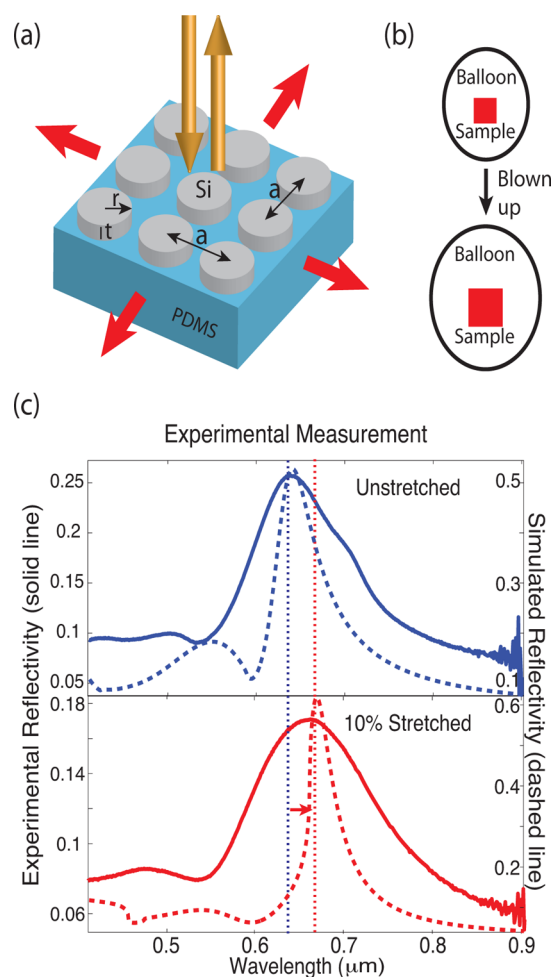
In order to achieve isotropic variation of the periodicity a, the PDMS sample must be stretched isotropically. To this end, the sample was fixed on a black balloon with radius R_1 (Figure 4b) much larger than the sample size. The balloon was then gradually expanded to R_2. Through this method, the periodicity of the sample was isotropically increased from a_1 to $a_2 = a_1 \cdot (R_2/R_1)$. The reflectance spectrum at normal incidence was measured with the same ultraviolet−visible photospectrometer as the one used to measure the static colors and is shown in Figure 4d. Compared with the RCWA simulation result (dashed line in Figure 4c), which was obtained using the measured refractive index dispersion of the deposited Si and assuming a constant rod radius, the spectral position of the experimental reflectance peaks and the simulated spectra match well. The spectral shift of the measured reflectance peak was 32 nm when the sample is stretched by approximately 10%. The magnitude of the measured reflectance is lower than simulated due to the fabrication inaccuracies mentioned above. Since the Si layer on PDMS was not quite flat after Si deposition, interference lithography was problematic: there was some variation in rod size over a length scale of a couple of periods,

together with a variation of the level of the rods, which could have had an adverse effect on the observation of Fano resonance. Also, the RIE of the Si layer and the mask layer removal by ashing might have damaged the PDMS surface to some extent and led to the formation of SiO_2 on the PDMS surface.

Because of those fabrication reasons, in the stretchable samples the Fano resonance can be best observed (with the experimental peak follows the simulated peak) when the stretching is less than 10%. However, we did not observe any degradation of the samples or their optical response after repeated stretching experiments. Another layer of PDMS spin-coated on top of the structure could also add additional stability to the structures during stretching. As mentioned before, it is possible to use different materials and other designs to achieve the same Fano resonance effect also in other wavelength regions. Very repeatable and controlled stretching mechanisms[4,38] are available. Therefore, we believe that a tunable spectral response over a wide wavelength regime could be achieved in a controlled and repeatable way using the proposed Fano resonance effect.

In this letter, we propose a structural color mechanism that uses the optical Fano resonance effect of light on a periodic surface structure. To this end, we have designed and fabricated a structure of periodic high-index rods on low-index substrates that show Fano resonance of the reflected and guided modes in the visible wavelength range. The predicted Fano resonance maxima were observed in the reflectance spectra on glass and PDMS substrates, with weak angular dependence. Moreover, dynamical color control was achieved by isotropically stretching the elastic PDMS substrates with the fabricated Fano structure, resulting in a shift of reflection peaks in agreement with simulation.

This mechanism for structural color and the geometry demonstrated is very versatile and can be specifically tailored for different applications, e.g., in displays or light emitting devices. In particular, the Q-factor and therefore the bandwidth of the resonance can be tuned to achieve a broad reflection bandwidth for displays or narrow reflectance bandwidth for light emitting or lasing applications. In addition, the designed structure shows good performance over a broad range of viewing angles.

The proposed method has the potential to lead the way to static and dynamic color control for a broad range of applications. The resonance effect achieved with these structures can be further optimized by improving the fabrication mechanism to achieve better accuracy and uniformity. Furthermore, the spectral range over which the effect and the reflectance color can be tuned could be extended by using materials that are lossless in the full visible spectrum, such as TiO_2 or Ta_2O_5.

■ ASSOCIATED CONTENT

Ⓢ Supporting Information

Angular dependence illustration. This material is available free of charge via the Internet at http://pubs.acs.org.

■ AUTHOR INFORMATION

Corresponding Author

*E-mail: ycshen@mit.edu. Phone: +1(617) 253 3887. Fax: +1 (617)-253-2562.

Author Contributions

[⊥]These authors contributed equally to the work.

Notes

The authors declare no competing financial interest.

■ REFERENCES

(1) Kinoshita, S.; Yoshioka, S.; Miyazaki, J. Physics of structural colors. *Rep. Prog. Phys.* **2008**, *71*, 076401.

(2) Graham-Rowe, D. Tunable structural colour. *Nat. Photonics* **2009**, *3*, 551−553.

(3) Kim, H.; Ge, J.; Kim, J.; Choi, S.-e.; Lee, H.; Lee, H.; Park, W.; Yin, Y.; Kwon, S. Structural colour printing using a magnetically tunable and lithographically fixable photonic crystal. *Nat. Photonics* **2009**, *3*, 534−540.

(4) Arsenault, A. C.; Puzzo, D. P.; Manners, I.; Ozin, G. A. Photonic-crystal full-colour displays. *Nat. Photonics* **2007**, *1*, 468−472.

(5) Prum, R. O.; Torres, R. H.; Williamson, S.; Dyck, J. Coherent light scattering by blue feather barbs. *Nature* **1998**, *396*, 28−29.

(6) Forster, J. D.; Noh, H.; Liew, S. F.; Saranathan, V.; Schreck, C. F.; Yang, L.; Park, J.-G.; Prum, R. O.; Mochrie, S. G.; O'Hern, C. S. Others, Biomimetic isotropic nanostructures for structural coloration. *Adv. Mater.* **2010**, *22*, 2939−2944.

(7) Noh, H.; Liew, S. F.; Saranathan, V.; Mochrie, S. G.; Prum, R. O.; Dufresne, E. R.; Cao, H. How noniridescent colors are generated by quasi-ordered structures of bird feathers. *Adv. Mater.* **2010**, *22*, 2871−2880.

(8) Kolle, M.; Zheng, B.; Gibbons, N.; Baumberg, J. J.; Steiner, U. Stretch-tuneable dielectric mirrors and optical microcavities. *Opt. Express* **2010**, *18*, 4356−4364.

(9) Kolle, M.; Salgard-Cunha, P. M.; Scherer, M. R.; Haung, F.; Vukusic, P.; Mahajan, S.; Baumberg, J. J.; Steiner, U. Mimicking the colourful wing scale structure of the Papilio blumei butterfly. *Nat. Nanotechnol.* **2010**, *5*, 511−515.

(10) Kolle, M.; Lethbridge, A.; Kreysing, M.; Baumberg, J. J.; Aizenberg, J.; Vukusic, P. Bio-inspired band-gap tunable elastic optical multilayer fibers. *Adv. Mater.* **2013**, *25*, 2239−2245.

(11) Joannopoulos, J.; Johnson, S.; Winn, J.; Meade, R. *Photonic Crystals: Molding the Flow of Light*, 2nd ed.; Princeton University Press: Princeton, NJ, 2011.

(12) Michaelis, B.; Snoswell, D. R.; Bell, N. A.; Spahn, P.; Hellmann, G. P.; Finlayson, C. E.; Baumberg, J. J. Generating lithographically-defined tunable printed structural color. *Adv. Eng. Mater.* **2013**, *15*, 948−953.

(13) Aschwanden, M.; Stemmer, A. Polymeric, electrically tunable diffraction grating based on artificial muscles. *Opt. Lett.* **2006**, *31*, 2610−2612.

(14) Macleod, H. A. *Thin-Film Optical Filters*; CRC Press: Boca Raton, FL, 2001.

(15) Yeh, P. *Optical Waves in Layered Media*; Wiley Series in Pure and Applied Optics; Wiley: New York, 2005.

(16) Kats, M. A.; Blanchard, R.; Genevet, P.; Capasso, F. Nanometre optical coatings based on strong interference effects in highly absorbing media. *Nat. Mater.* **2013**, *12*, 20−24.

(17) Xu, T.; Wu, Y.-K.; Luo, X.; Guo, L. J. Plasmonic nanoresonators for high-resolution colour filtering and spectral imaging. *Nat. Commun.* **2010**, *1*, 59.

(18) Tan, S. J.; Zhang, L.; Zhu, D.; Goh, X. M.; Wang, Y. M.; Kumar, K.; Qiu, C.-W.; Yang, J. K. Plasmonic color palettes for photorealistic

printing with aluminum nanostructures. *Nano Lett.* **2014**, *14*, 4023−4029.

(19) Si, G.; Zhao, Y.; Lv, J.; Lu, M.; Wang, F.; Liu, H.; Xiang, N.; Huang, T. J.; Danner, A. J.; Teng, J. Reflective plasmonic color filters based on lithographically patterned silver nanorod arrays. *Nanoscale* **2013**, *5*, 6243−6248.

(20) Olson, J.; Manjavacas, A.; Liu, L.; Chang, W.-S.; Foerster, B.; King, N. S.; Knight, M. W.; Nordlander, P.; Halas, N. J.; Link, S. Vivid, full-color aluminum plasmonic pixels. *Proc. Natl. Acad. Sci. U.S.A.* **2014**, *111*, 14348−14353.

(21) Kumar, K.; Duan, H.; Hegde, R. S.; Koh, S. C.; Wei, J. N.; Yang, J. K. Printing colour at the optical diffraction limit. *Nat. Nanotechnol.* **2012**, *7*, 557−561.

(22) Liu, Y. J.; Si, G. Y.; Leong, E. S. P.; Xiang, N.; Danner, A. J.; Teng, J. H. Light-driven plasmonic color filters by overlaying photoresponsive liquid crystals on gold annular aperture arrays. *Adv. Mater.* **2012**, *24*, OP131−OP135.

(23) Yokogawa, S.; Burgos, S. P.; Atwater, H. A. Plasmonic color filters for CMOS image sensor applications. *Nano Lett.* **2012**, *12*, 4349−4354.

(24) Chen, Q.; Cumming, D. R. High transmission and low color cross-talk plasmonic color filters using triangular-lattice hole arrays in aluminum films. *Opt. Express* **2010**, *18*, 14056−14062.

(25) Miroshnichenko, A. E.; Flach, S.; Kivshar, Y. S. Fano resonances in nanoscale structures. *Rev. Mod. Phys.* **2010**, *82*, 2257.

(26) Fan, S.; Joannopoulos, J. Analysis of guided resonances in photonic crystal slabs. *Phys. Rev. B* **2002**, *65*, 235112.

(27) Fan, S.; Suh, W.; Joannopoulos, J. Temporal coupled-mode theory for the Fano resonance in optical resonators. *J. Opt. Soc. Am. A* **2003**, *20*, 569−572.

(28) Liu, V.; Fan, S. S^4: A free electromagnetic solver for layered periodic structures. *Comput. Phys. Commun.* **2012**, *183*, 2233−2244.

(29) Kunz, K. S.; Luebbers, R. J. *The Finite Difference Time Domain Method for Electromagnetics*; CRC Press: Boca Raton, FL, 1993.

(30) Mandelshtam, V. A.; Taylor, H. S. Harmonic inversion of time signals and its applications. *J. Chem. Phys.* **1997**, *107*, 6756−6769.

(31) Shen, Y.; Ye, D.; Celanovic, I.; Johnson, S.; Joannopoulos, J.; Soljačić, M. *Science* **2014**, *343*, 1499−1501.

(32) Hsu, C. W.; Zhen, B.; Qiu, W.; Shapira, O.; DeLacy, B.; Joannopoulos, J.; Soljačić, M. *Nat. Commun.* **2014**, *5*, 3152.

(33) Schattenburg, M.; Aucoin, R.; Fleming, R. Optically matched trilevel resist process for nanostructure fabrication. *J. Vac. Sci. Technol. B* **1995**, *13*, 3007−3011.

(34) Savas, T.; Schattenburg, M.; Carter, J.; Smith, H. I. Large-area achromatic interferometric lithography for 100 nm period gratings and grids. *J. Vac. Sci. Technol. B* **1996**, *14*, 4167−4170.

(35) Walsh, M. E. On the design of lithographic interferometers and their application. Ph.D. thesis, Massachusetts Institute of Technology, 2004.

(36) Anderson, E. H. Fabrication and electromagnetic applications of periodic nanostructures. Ph.D. thesis, Massachusetts Institute of Technology, 1988.

(37) Schattenburg, M.; Anderson, E.; Smith, H. I. X-ray/VUV transmission gratings for astrophysical and laboratory applications. *Phys. Scr.* **1990**, *41*, 13.

(38) Kamita, G.; Kolle, M.; Huang, F.; Baumberg, J. J.; Steiner, U. Multilayer mirrored bubbles with spatially-chirped and elastically-tuneable optical bandgaps. *Opt. Express* **2012**, *20*, 6421−6428.